ISSN 0915-633X

NATIONAL INSTITUTE FOR FUSION SCIENCE

Large Potential Change Induced by Pellet Injection in JIPP T-IIU Tokamak Plasmas

Y. Hamada, K.N. Sato, H. Sakakita, A. Nishizawa, Y. Kawasumi, R. Liang, K. Kawahata, A. Ejiri, K. Toi, K. Narihara, K. Sato, T. Seki, H. Iguchi, A. Fujisawa, K. Adachi, S. Hidekuma, S. Hirokura, K. Ida, M. Kojima, J. Koong, R. Kumazawa, H. Kuramoto, T. Minami,. M. Sasao, T. Tsuzuki, J.Xu, I. Yamada, and T. Watari

(Received - Apr. 28, 1995)

NIFS-357 May 1995

RESEARCH REPORT
NIFS Series

NAGOYA, JAPAN

Large Potential Change induced by Pellet Injection in JIPP T-IIU Tokamak Plasmas

Y. Hamada, K. N. Sato, H. Sakakita*, A. Nishizawa, Y. Kawasumi, R. Liang, K. Kawahata, A. Ejiri, K. Toi, K. Narihara, K. Sato, T. Seki, H. Iguchi, A. Fujisawa, K. Adachi, S. Hidekuma, S. Hirokura, K. Ida, M. Kojima, J. Koong, R. Kumazawa, H. Kuramoto, T. Minami, M. Sasao, T. Tsuzuki, J. Xu, I. Yamada, T. Watari

National Institute for Fusion Science , Nagoya, 464-01 , Japan.

* *Department of Aerospace Engineering, Nagoya University , Nagoya $64-01 , Japan .*

A large, rapid change in the local plasma potential is found to be induced by off-axis hydrogen ice-pellet injection into a tokamak plasma. The polarity of the rapid change is reversed when the pellet is injected into the upper and lower halves of the poloidal plasma cross-section. This change can be interpreted as being due to the gradient-B drift of particles in the high-density plasmas of the pellet cloud, before the increase of the plasma density due to the ablation becomes uniform on the magnetic surface.

Key words: tokamak, pellet injection, HIBP, potential, beam, ablation.

Hydrogen ice-pellet injection into a tokamak plasma is one of the most important methods for fueling, controlling the density profile, and improving the confinement of a tokamak plasma.[1-8] In addition, the interaction of pellets with a high-temperature tokamak plasma induces interesting phenomena like striation[3,6], rapid pre-cooling[3,5], "snake" oscillation[4], and large tail formation[8], which have been studied by various diagnostics. In the present paper, observations of the large potential change induced by pellet injection into a tokamak plasma are presented. This study is the first to examine the electric field resulting from pellet injection by a heavy ion beam probe (HIBP). Plasma's equilibrium potential is negative with respect to the vacuum chamber and exhibits a large deviation from neoclassical theory.[9,10] The origin of this potential is not clear. A large potential gradient at the plasma surface is also considered to be the origin of H-mode in tokamak plasmas. To clarify experimentally the mechanism that produces the potential in a toroidal plasmas is, therefore, very important.

The experiment was performed with the JIPP T-IIU tokamak. Its major radius is 93 cm and the maximum toroidal field is 3 Tesla.[11] The experiment was conducted at a relatively low density of about $2 \times 10^{13}/cm^3$ so that beam penetration into the center of the plasma could be obtained. A 450 keV singly-charged thallium ion beam (primary beam) is injected into the tokamak as a heavy ion beam probe (HIBP).[10] The intensity and energy of a secondary beam (Tl^{++}) produced in the tokamak plasma was measured with a parallel plate analyzer in order to study the local density and local potential. The HIBP setup is similar to that in the TEXT tokamak[12].

Figure 1a shows injected thallium beam trajectories in the tokamak plasma, and points of measurement (sample volume) discussed in this paper. When primary ions (Tl^{+}) are injected into the tokamak along the trajectory A of Fig. 1a, only the secondary ions (Tl^{++}) generated at position A, out of all those generated along the whole trajectory inside the plasma, go through the entrance slit of a parallel-plate energy analyzer and hit the upper and lower detector plates placed at the focal point. We can sweep this point of the measurement (sample volume) by sweeping the injection angle of the primary beam to the tokamak as shown in Fig. 1a.

The basic principle of potential measurement by HIBP was proposed by R.L.Hickok et al.[13] and is illustrated in Fig. 1b. The energy of the secondary ions detected at the energy analyzer differs from the initial beam energy by $e\Phi(r_X)$, where $\Phi(r_X)$ is the local plasma potential at an ionization point X, because energy conservation for primary and secondary ions holds respectively, as is illustrated in Fig. 1b. The change of the energy due to an electric field caused by the time derivative of a vector potential (dA/dt), is small even in the MHD time scale, since for low ß plasmas such as tokamak plasmas, A is parallel to the equilibrium magnetic field [14] and is nearly perpendicular to the trajectory of the primary beam that is injected almost perpendicularly to the magnetic field. The change in the beam energy even at the MHD time scale is then due to the electrostatic potential at the ionization point.

The current-profile change during pellet injection, however, will induce a change in the beam's toroidal deflection angle and in the out-of-plane entrance angle ($\delta\omega_{en}$) to the analyzer. Since a parallel-plate analyzer measures the energy of the movement parallel to the analyzer plane (the plane of symmetry of the analyzer), instead of the total kinetic

energy, the current-profile change results in an error of $-\delta\{V_b \sin^2(\omega_{en})\} = -2V_b \cos(\omega_{en,0}) \sin(\omega_{en,0}) \delta\omega_{en}$ in the potential measurement. Here, V_b is the primary beam energy and $\omega_{en,0}$ is the out-of plane entrance angle before the injection. Since this error changes sign as $\omega_{en,o}$ changes sign, we can estimate the magnitude of this error by rotating the analyzer on the vertical axis, which changes $\omega_{en,o}$.

The small change in the energy compared to the original energy is measured by the normalized difference (ND) of secondary beam currents to the upper and lower detector plates (I_u, I_d), where $ND = (I_u - I_d)/(I_u + I_d)$. [10,15] The conversion rate of ND to the change in plasma potential is about 1.8 kV/ND for a 450 keV beam.

Figure 1a also schematically illustrates the mechanism of a injection-angle-control of the hydrogen pellet injector. By changing the angle of the guide tube, on-axis (purely horizontal) and off-axis(upwards and downwards) injections of an ice-pellet are conducted.[8]

Figure 2 shows typical rapid changes of the potential when a hydrogen pellet is injected (a) slightly downwards, (b) purely horizontally into the center of the tokamak plasma, and (c) slightly upwards, as illustrated in Fig. 1a. Table 1 lists the injection angles and the positions of the maximum ablation for these three cases. The potential is measured at sample volume A of Fig. 1a, which is near $r/a_p = 0.1$ and is inside the magnetic surface of the pellet ablation. The photographs of the ablation cloud in these cases show that the ablation clouds lie on a straight line and do not show curved trajectories or the large tail (the tail mode).[8] Plasma current is about 150 kA (q_a=6). As shown in Fig. 2, the reactions on the plasma potential are characterized by the very large, sharp increase and decrease. With off-axis injection, the potential changes occur roughly

simultaneously with the rise of the $H\alpha$ light of the pellet ablation monitor. The sign of the potential change is positive for the case of downward injection and negative for upward injection. The maximum absolute value of the change occurs near the end of the ablation. For the case of pure horizontal injection, the potential behaviour is very different, In contrast to off-axis injection, the change in potential during ablation is very small. After the ablation process is completed, the potential starts to go negative.

The error in the rapid measurement of the potential by the HIBP may be caused by a beam deflection due to the change in the plasma current profile. We tested for the error by rotating the analyzer on the vertical axis on different shots, which changes the secondary beam's out-of-plane entrance angles in the analyzer. Since the results are similar to those in Fig. 2 for various rotation angles, we conclude that the error is small. In addition, it is found that the beam's toroidal position on the detector plates does not move during the ablation. This may mean that the current profile change may start after the ablation ends.

Figure 3 shows upwards off-axis injection data from sample volume B of Fig. 1b, which is at $r/a_p = 0.6$ and is outside the maximum ablation radius. ND (potential), the sum of detector currents and $H\alpha$ light ablation monitor are shown. The pellet injection system and HIBP apparatus are separated by a toroidal angle of 144 degrees. Figure 3 clearly shows that the maximum absolute change of the potential at B occurs before the maximum ablation of the pellet in contrast to Fig. 2. In addition, the rise and subsequent decay of the sum signal is observed in contrast to Fig. 2 and the space potential change occurs before the change of the sum signal.

The sum of the detector current (intensity of the secondary current at the detector) is described by the following equation,

$$I_s=\sigma_{1,2}\, n_e(r_B)\, I_{bo} \exp\{-\int_{a_p}^{r_B} \sigma_{1,2}\, n_e(\rho)d\rho\} \exp\{-\int_{r_B}^{a_p} \sigma_{2,3}\, n_e(\rho)d\rho\}, \qquad (1)$$

where I_{bo} is the intensity of the Tl^{1+} injected beam and r_B is the point of measurement respectively, and $\sigma_{i,j}$ is the cross-section for ionization of Tl by the plasma from the i-th ionization state to the j-th ionization state. The integration is from plasma boundary to sample volume B along the primary beam trajectory and from B to plasma boundary along the secondary beam trajectory. a_p denotes plasma boundary. The change in the potential shown in Fig. 3 and also in Fig. 2a and 2c occurs prior to the change in the intensity of the secondary beam at the detector. This fact means that the potential perturbation travels toroidally to the HIBP section much faster than the density perturbation, since the intensity of the secondary beam (sum) changes when the plasma density changes. This may be reasonable because the potential perturbation in this case may propagate with a speed comparable to that of high-temperature thermal electrons, while the expansion of the pellet blob propagates with the speed of the ion thermal velocity of the pellet blob. The central temperature is about 1.2 keV before the injection and the temperature drops by about 60% at about the ablated magnetic surface.

From equation 1, it is considered that the increase in the sum, followed by a decrease as shown in Fig. 3, is caused by an increase in the density at the sample volume $n_e(r_B)$ due to the expansion of the ablation cloud in the toroidal direction, while the subsequent decrease of the sum signal is caused by increased beam attenuation due to an increase of the density along the trajectories. In all cases of Figure 2, we observe only a

decay of the sum signals during the ablation, since the ablation points are outside the magnetic surface of sample volume A. These facts also suggest that the increase of the sum signal is due to that of the plasma density at the sample volume.

The changes of the potential with off-axis injections can be explained in the following manner. The high-density blob produced by downward pellet injection stays for a short duration in the lower portion of the magnetic surface while expanding toroidally. Because of the gradient-B drifts (curvature drifts) of ions and electrons in the high-density blob, charge separation occurs vertically; in this case, radially. It is impossible for high temperature electrons to compensate the charge separation, since it occurs radially, that is, across the different magnetic surfaces. It should be noted that the potential tends to be constant on the magnetic surface (surface quantity), because the potential perturbation propagates very rapidly. Since the measured potential is an integral of the electric field from the vacuum vessel to the sample volume, it is sensitive to the generation of the radial electric field outside the magnetic surface on which the sample volume is located. It is insensitive to the radial electric field inside the magnetic surface of the sample volume. This explains why in the cases in Fig. 2a and 2c we observe the large potential changes even though the pellet does not penetrate to sample volume A and why we observe small and early potential change in Fig. 3 at sample volume B.

The order of magnitude of this potential may be estimated by the following consideration. Let us assume that the pellet is deposited at a minor radius of r_{pl} and at a poloidal angle of θ_{pl}. The pellet cloud has a depth of L_{pl} across the magnetic surface and an area of S_{pl} along the magnetic surface. It has an averaged plasma density of $n_{e,pellet}$, and an

average temperature of T_{pellet}. The amount of charge accumulation dQ/dt, across the magnetic surfaces is given by $dQ/dt = j_{drift} \cdot S_{pl} \cdot \sin(\theta_p)$, where j_{drift} is the vertical current induced by the gradient-B drift of the pellet cloud. j_{drift} can be expressed as $j_{drift} = n_{e,pellet} \cdot 2kT_{pellet}/(m_e \cdot R_{pl} \cdot \omega_{ce})$, where R_{pl} is the major radius of the dominant ablation point in the plasma. We model the potential formation as charging by j_{drift} a parallel plate capacitor with an area of magnetic surface and a plate separation given by L_{pl}. The capacitance is $C_p = \varepsilon_o \cdot \varepsilon_p (2\pi R_p 2\pi r_{pl}) / L_{pl}$, where ε_p is the plasma dielectric constant. Since ε_p is expressed by $\varepsilon_p = 1 + (\omega_{pi}/\omega_{ci})^2$, it is proportional to the plasma density. The capacitance is then dominated by the contribution from the pellet cloud for the case that the number of total deposited particles is higher than that of the original particles located between the magnetic surfaces which are separated by L_{pl}. This case is experimentally supported by the fact that the fast ECE temperature drops to less than half at our pellet injection. In this case $C_p \cong \varepsilon_o \cdot \varepsilon_p \cdot S_{pl} / L_{pl}$. The rate of potential change at the magnetic surface inside the ablation region is $d\Phi_p/dt = (dQ/dt) / C_p$ and can be simply described by

$$\frac{d\Phi_p}{dt} \cong \frac{2L_{pl}}{R_{pl}} \frac{kT_{pellet}}{e} \omega_{ci} \sin(\theta_p). \qquad (2)$$

The gradient-B drift can explain the polarity of the potential change for off-axis injection through the dependence on $\sin(\theta p)$. Table 1 shows the various parameters associated with the pellet injections for the cases in Fig. 2. We measured the thickness of the ablation cloud L_{pl} by the rapid decrease of multichannel ECE signals during pellet injection, assuming that the electron energy on the given magnetic surface remains nearly

constant before radial heat diffusion becomes dominant. Theoretical analysis and experimental measurements have determined that the temperature of the pellet cloud is a few eV.[4,6,17,18] If we assume that the temperature of pellet cloud is 2 eV, the predicted values of the rate of the potential change are about one order of magnitude larger than the observed values, as shown in Table 1. This difference may be explained by several factors. One is the fact that the very high density part of the plasma blob is so collisional that it may not effectively contribute to the charge separation due to the gradient B drift. The high temperature portion of the plasma blob tends to become rapidly uniform on the magnetic surface and does not effectively contribute to the formation of the potential. Accordingly, it is very difficult to obtain better agreement between the observed and predicted changes of the plasma potential without a very extensive measurement of the pellet plasma expansion.

When the hydrogen pellet is injected horizontally towards the center of the plasma cross-section, the deposited high-density blob is unable to generate a potential, since the gradient-B drift is parallel to the magnetic surface. This explains why in Fig. 2b, the change of potential during the ablation is negligible. After the ablation is completed, the change in potential becomes negative. The high density blob created by the pellet usually expands in both directions along the magnetic lines of force. The negative voltage after the ablation is completed in Fig. 2b may mean that the direction of the dominant expansion along the magnetic lines of force is parallel to the toroidal rotation of the ohmic plasma, i. e. anti-parallel to the plasma current because of the interaction with the plasma rotation. In this case, the induced potential would be negative, since the dominant part of the plasma blob is in the upper part of the poloidal cross-section.

Since the charge separation to produce such a fast change of the space potential is small, the formation of the fast potential change will be rapidly restored to zero when this mechanism of charge separation is stopped. The short life time of the negative potential may be explained in this way.

In summary, a fast potential change produced by pellet injection into a tokamak plasma is observed and explained by the gradient-B drift induced charge separation in the high-density plasma blob before it can expand along the magnetic surfaces.

The authors thank visiting professor of our institute, Dr. T. P. Crowley of Rensselaer Polytechnic Institute for his critical reading of the manuscript. We also wish to thank Director-General of the National Institute for Fusion Science, Prof. A. Iiyoshi, and Professors M. Fujiwara and K. Matsuoka for their continuous support.

References

1) S. L. Milora, C. A. Forster, and P. H. Edmonds, Phys. Rev. Lett. **42**, 97 (1979).

2) S. L. Milora et al., Nuclear Fusion **20**, 1491 (1980).

3) TFR Group, Nuclear Fusion **27**, 1975 (1987).

4) A. Weller et al., Phys. Rev. Lett. **59**, 2303 (1987).

5) M. Sakamoto et al., Plasma Phys. Controlled Fusion **33**, 583 (1991).

6) R. D. Durst et al., Nuclear Fusion **30**, 3 (1990).

7) JET Team , in *Proceedings of the 13h International Conference on Plasma Physics and Conrolled Nuclear Fusion Research, Washington D.C., 1990* (IAEA, Vienna), Vol.1, p.27 (1991).

8) H. Sakakita et al., in *Proceedings of the 21th European Conference on Conrolled Fusion and Plasma Physics, (European Physical Society, Montpellier, 1994),* Part 1, p. 310.

9) X. Z. Yang et al., Phys. Fluids B **3**, 3448 (1991).

10)Y. Hamada et al., Plasma Phys. Controlled Fusion **36**, 1050 (1994).

11)K. Toi et al., in *Proceedings of the 14h International Conference on Plasma Physics and Conrolled Nuclear Fusion Research, Wurzburg, 1992* (IAEA, Vienna),Vol.1, p.301 (1993).

12)P. M. Schoch, J. C. Forster, W. C. Jennings, and R. L. Hickok, Rev. Sci. Instrum. **57**, 1825 (1986).

13)F. C. Jobes and R. L. Hickok, Nuclear Fusion **10**, 195 (1970).

14)for example, B. B. Kadomtsev and O. P. Pogutse, in Review of Plasma Physics, (Consultants Bureau, New York, 1970), Vol.5, p. 284.

15)L. Solensten and K. A. Connor, Rev. Sci. Instrum. **58**, 516 (1987).

16)P. B. Parks, R. J. Turnbull and C. A. Foster, Nuclear Fusion **17**, 539 (1977).

17)P. B. Parks and R. J. Turnbull, Phys. Fluids **21**, 1735 (1978).

18)P. B. Parks, Nuclear Fusion **20**, 311 (1980).

Figure Captions

Figure 1. a) Trajectories of primary (450 keV, Tl^+) and secondary (Tl^{++}) beams and points of ionization (measurement) A, B in JIPP T-IIU tokamak plasmas. Toroidal field is 3T. A schematic illustrating a guide tube of the pellet injection system which allows on-axis and off-axis pellet

injection is also shown. b) Behaviour of the energy (total and kinetic) of ions injected and ionized in a plasma along the ion trajectory. This schematic illustrates the basic principle of potential measurement in a plasma by a heavy ion beam probe. The energy of the secondary ions outside the plasma changes by an amount equal to the electron charge times the local plasma potential where the ionization from Tl^+ to Tl^{++} takes place. r_x is the position of the ionization. The solid line for beam energy shows kinetic beam energy, while the dotted line shows total beam energy.

Figure 2. Typical change of plasma potential (in terms of ND) measured by a heavy ion beam probe at sample volume A in Fig. 1a (solid line), in terms of ND, sum of the upper and lower plate-detector currents (dashed line, 0.1μA/1.0) and H_α light as a monitor of a pellet ablation (dotted line, arbitrary). The conversion from ND to the change of plasma potential is about 1.8 kV/1.0ND. ND is the difference between the upper and lower detector currents normalized by the sum and is proportional to the plasma potential. (a) is for off-axis downwards injection, (b) for horizontal (on-axis) injection, and (c) for off-axis upwards injection.

Figure 3. Fast time evolution of ND (potential,1.8 kV/1.0) in the lower trace, the intensity of the secondary beam to the detector (sum of the detector currents, 0.1μA/1.0) in the middle trace, and H_α light from pellet ablation monitor in the upper trace (arbitrary), measured at the observation point B in Fig. 1a. The injection is upwards with an angle of 4 degrees.

Table 1

Injection parameters of the hydrogen pellets and comparison of the rate of the potential change in the case of Fig. 2. The theoretical rate of the potential change is calculated by the equation 2. T_{pellet}= 2 eV is assumed.

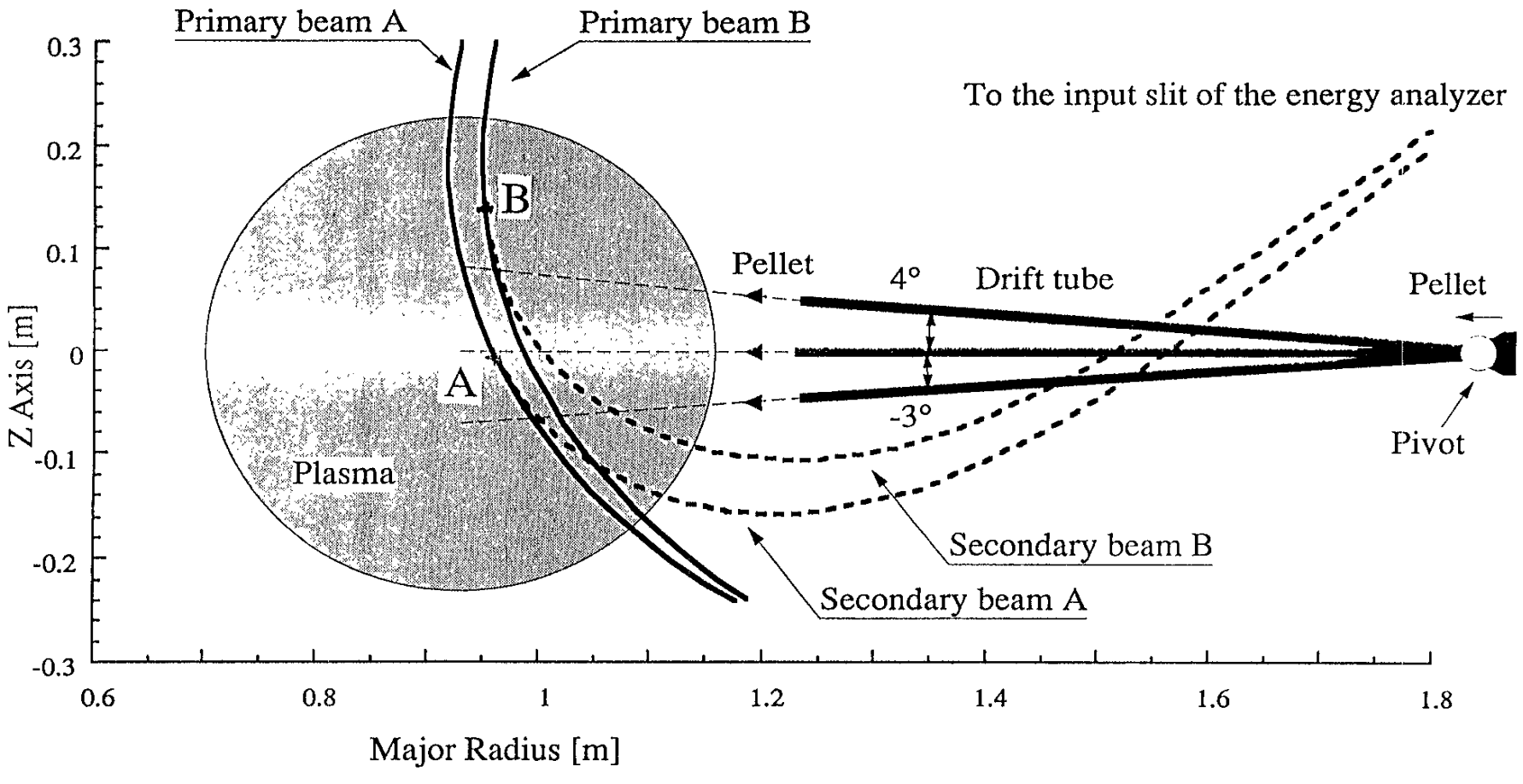
Primary beam A
Primary beam B
To the input slit of the energy analyzer
B
A
Pellet
4°
Drift tube
Pellet
-3°
Pivot
Plasma
Secondary beam B
Secondary beam A
Z Axis [m]
0.3
0.2
0.1
0
-0.1
-0.2
-0.3
0.6
0.8
1
1.2
1.4
1.6
1.8
Major Radius [m]

Figure 1a

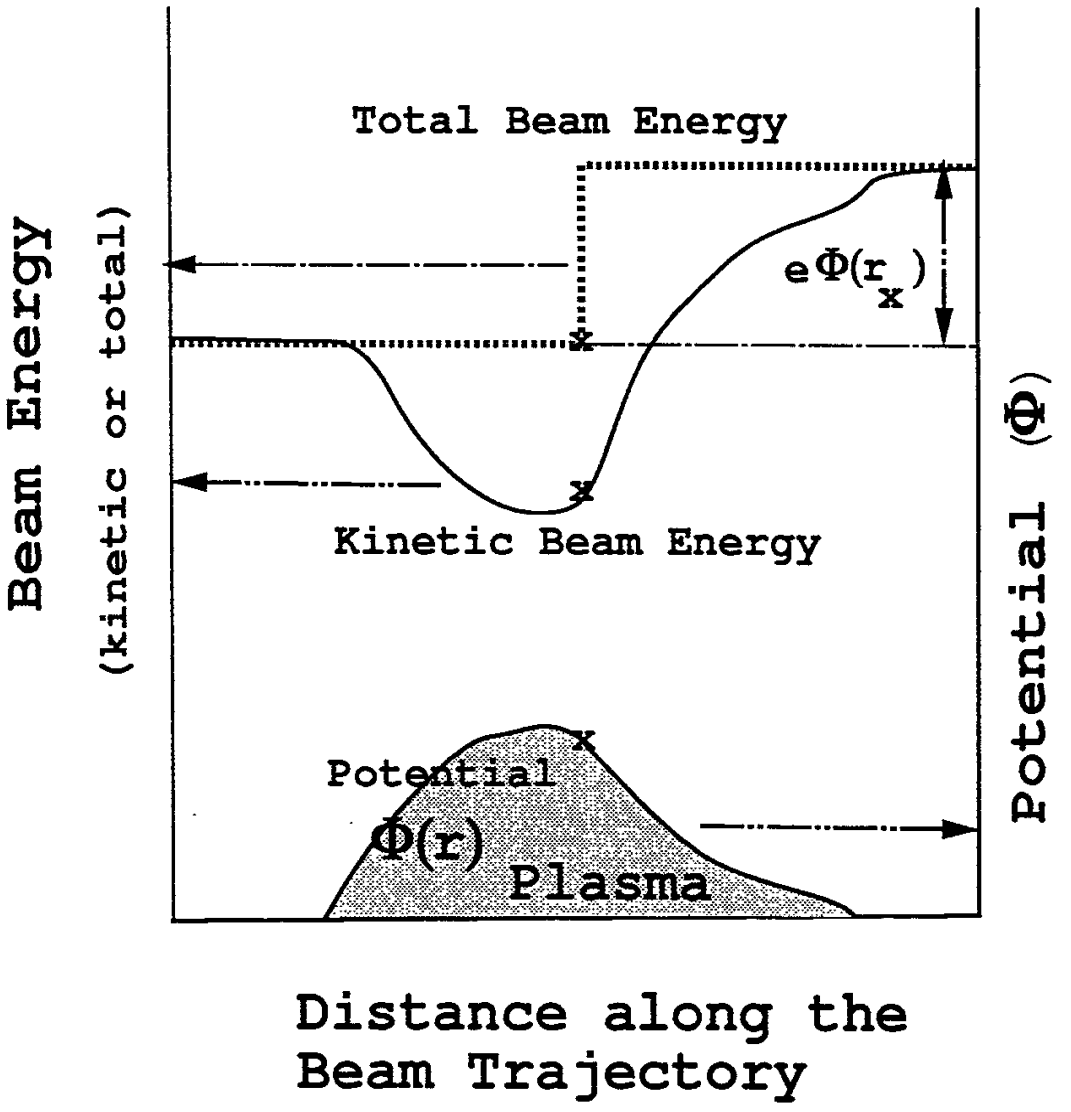
Total Beam Energy
eΦ(r x)
Beam Energy
(kinetic or total)
Kinetic Beam Energy
Potential (Φ)
Potential
Φ(r)
Plasma
Distance along the
Beam Trajectory

Figure 1b

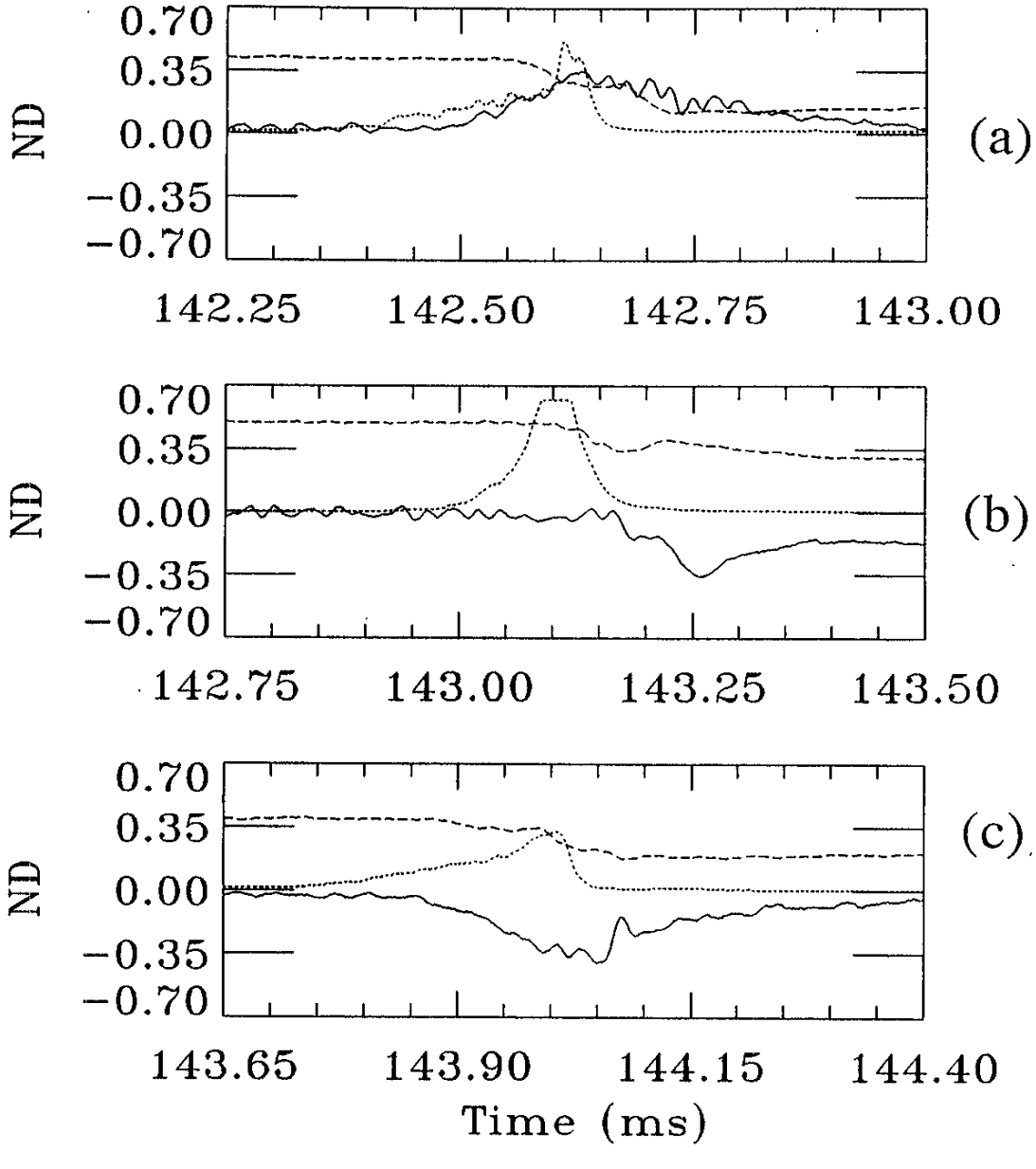
0.70
0.35
0.00
−0.35
−0.70
ND
142.25
142.50
142.75
143.00
(a)
142.75
143.00
143.25
143.50
(b)
143.65
143.90
144.15
144.40
(c)
Time (ms)

Figure 2

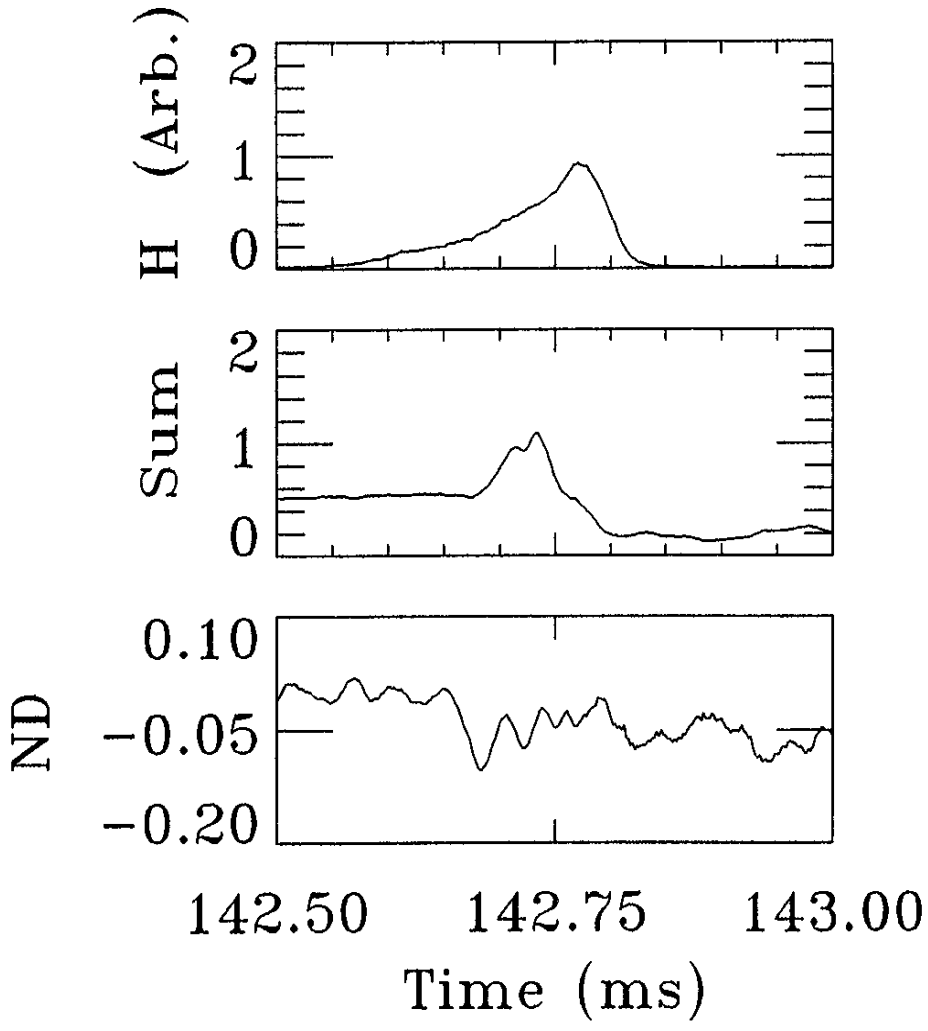

Figure 3

Parameters \ Shot Number	#70501	#70430	#70506
Injection angle [Degree]	- 3.0	0	+ 4.0
L_{pl} [cm]	6	6	6
r_{pl} [cm]	7.4	10.0	9.8
θ_{pl} [Degree]	- 66.0	0	+ 66.0
$d\Phi/dt$ (Theory) [V/Sec]	6.5×10^7	0	-6.4×10^7
$d\Phi/dt$ (Observed) [V/Sec]	5×10^6	0	-3.9×10^6

Table 1

Recent Issues of NIFS Series

NIFS-307 Y. Takeiri, A. Ando, O. Kaneko, Y. Oka, K. Tsumori, R. Akiyama, E. Asano, T. Kawamoto, T. Kuroda, M. Tanaka and H. Kawakami,
Development of an Intense Negative Hydrogen Ion Source with a Wide-Range of External Magnetic Filter Field; Sep. 1994

NIFS-308 T. Hayashi, T. Sato, H.J. Gardner and J.D. Meiss,
Evolution of Magnetic Islands in a Heliac; Sep. 1994

NIFS-309 H. Amo, T. Sato and A. Kageyama,
Intermittent Energy Bursts and Recurrent Topological Change of a Twisting Magnetic Flux Tube; Sep.1994

NIFS-310 T. Yamagishi and H. Sanuki,
Effect of Anomalous Plasma Transport on Radial Electric Field in Torsatron/Heliotron; Sep. 1994

NIFS-311 K. Watanabe, T. Sato and Y. Nakayama,
Current-profile Flattening and Hot Core Shift due to the Nonlinear Development of Resistive Kink Mode; Oct. 1994

NIFS-312 M. Salimullah, B. Dasgupta, K. Watanabe and T. Sato,
Modification and Damping of Alfvén Waves in a Magnetized Dusty Plasma; Oct. 1994

NIFS-313 K. Ida, Y. Miura, S -I. Itoh, J.V. Hofmann, A. Fukuyama, S. Hidekuma, H. Sanuki, H. Idei, H. Yamada, H. Iguchi, K. Itoh,
Physical Mechanism Determining the Radial Electric Field and its Radial Structure in a Toroidal Plasma; Oct. 1994

NIFS-314 Shao-ping Zhu, R. Horiuchi, T. Sato and The Complexity Simulation Group,
Non-Taylor Magnetohydrodynamic Self-Organization; Oct. 1994

NIFS-315 M. Tanaka,
Collisionless Magnetic Reconnection Associated with Coalescence of Flux Bundles; Nov. 1994

NIFS-316 M. Tanaka,
Macro-EM Particle Simulation Method and A Study of Collisionless Magnetic Reconnection; Nov. 1994

NIFS-317 A. Fujisawa, H. Iguchi, M. Sasao and Y. Hamada,
Second Order Focusing Property of 210° Cylindrical Energy Analyzer; Nov. 1994

NIFS-318 T. Sato and Complexity Simulation Group,
Complexity in Plasma - A Grand View of Self- Organization; Nov. 1994

NIFS-319 Y. Todo, T. Sato, K. Watanabe, T.H. Watanabe and R. Horiuchi,
MHD-Vlasov Simulation of the Toroidal Alfvén Eigenmode; Nov. 1994

NIFS-320 A. Kageyama, T. Sato and The Complexity Simulation Group,
Computer Simulation of a Magnetohydrodynamic Dynamo II: Nov. 1994

NIFS-321 A. Bhattacharjee, T. Hayashi, C.C.Hegna, N. Nakajima and T. Sato,
Theory of Pressure-induced Islands and Self-healing in Three-dimensional Toroidal Magnetohydrodynamic Equilibria; Nov. 1994

NIFS-322 A. Iiyoshi, K. Yamazaki and the LHD Group,
Recent Studies of the Large Helical Device; Nov. 1994

NIFS-323 A. Iiyoshi and K. Yamazaki,
The Next Large Helical Devices; Nov. 1994

NIFS-324 V.D. Pustovitov
Quasisymmetry Equations for Conventional Stellarators; Nov. 1994

NIFS-325 A. Taniike, M. Sasao, Y. Hamada, J. Fujita, M. Wada,
The Energy Broadening Resulting from Electron Stripping Process of a Low Energy Au^- Beam; Dec. 1994

NIFS-326 I. Viniar and S. Sudo,
New Pellet Production and Acceleration Technologies for High Speed Pellet Injection System "HIPEL" in Large Helical Device; Dec. 1994

NIFS-327 Y. Hamada, A. Nishizawa, Y. Kawasumi, K. Kawahata, K. Itoh, A. Ejiri, K. Toi, K. Narihara, K. Sato, T. Seki, H. Iguchi, A. Fujisawa, K. Adachi, S. Hidekuma, S. Hirokura, K. Ida, M. Kojima, J. Koong, R. Kumazawa, H. Kuramoto, R. Liang, T. Minami, H. Sakakita, M. Sasao, K.N. Sato, T. Tsuzuki, J. Xu, I. Yamada, T. Watari,
Fast Potential Change in Sawteeth in JIPP T-IIU Tokamak Plasmas; Dec. 1994

NIFS-328 V.D. Pustovitov,
Effect of Satellite Helical Harmonics on the Stellarator Configuration; Dec. 1994

NIFS-329 K. Itoh, S-I. Itoh and A. Fukuyama,
A Model of Sawtooth Based on the Transport Catastrophe; Dec. 1994

NIFS-330 K. Nagasaki, A. Ejiri,
Launching Conditions for Electron Cyclotron Heating in a Sheared Magnetic Field; Jan. 1995

NIFS-331 T.H. Watanabe, Y. Todo, R. Horiuchi, K. Watanabe, T. Sato,
An Advanced Electrostatic Particle Simulation Algorithm for Implicit Time Integration; Jan. 1995

NIFS-332 N. Bekki and T. Karakisawa,
Bifurcations from Periodic Solution in a Simplified Model of Two-dimensional Magnetoconvection; Jan. 1995

NIFS-333 K. Itoh, S.-I. Itoh, M. Yagi, A. Fukuyama,
Theory of Anomalous Transport in Reverse Field Pinch; Jan. 1995

NIFS-334 K. Nagasaki, A. Isayama and A. Ejiri
Application of Grating Polarizer to 106.4GHz ECH System on Heliotron-E; Jan. 1995

NIFS-335 H. Takamaru, T. Sato, R. Horiuchi, K. Watanabe and Complexity Simulation Group,
A Self-Consistent Open Boundary Model for Particle Simulation in Plasmas; Feb. 1995

NIFS-336 B.B. Kadomtsev,
Quantum Telegragh : is it possible?; Feb. 1995

NIFS-337 B.B.Kadomtsev,
Ball Lightning as Self-Organization Phenomenon; Feb. 1995

NIFS-338 Y. Takeiri, A. Ando, O. Kaneko, Y. Oka, K. Tsumori, R. Akiyama, E. Asano, T. Kawamoto, M. Tanaka and T. Kuroda,
High-Energy Acceleration of an Intense Negative Ion Beam; Feb. 1995

NIFS-339 K. Toi, T. Morisaki, S. Sakakibara, S. Ohdachi, T.Minami, S. Morita, H. Yamada, K. Tanaka, K. Ida, S. Okamura, A. Ejiri, H. Iguchi, K. Nishimura, K. Matsuoka, A. Ando, J. Xu, I. Yamada, K. Narihara, R. Akiyama, H. Idei, S. Kubo, T. Ozaki, C. Takahashi, K. Tsumori,
H-Mode Study in CHS; Feb. 1995

NIFS-340 T. Okada and H. Tazawa,
Filamentation Instability in a Light Ion Beam-plasma System with External Magnetic Field; Feb. 1995

NIFS-341 T. Watanbe, G. Gnudi,
A New Algorithm for Differential-Algebraic Equations Based on HIDM; Feb. 13, 1995

NIFS-342 Y. Nejoh,
New Stationary Solutions of the Nonlinear Drift Wave Equation; Feb. 1995

NIFS-343 A. Ejiri, S. Sakakibara and K. Kawahata,
Signal Based Mixing Analysis for the Magnetohydrodynamic Mode Reconstruction from Homodyne Microwave Reflectometry; Mar.. 1995

NIFS-344 B.B.Kadomtsev, K. Itoh, S.-I. Itoh
Fast Change in Core Transport after L-H Transition; Mar. 1995

NIFS-345 W.X. Wang, M. Okamoto, N. Nakajima and S. Murakami,
An Accurate Nonlinear Monte Carlo Collision Operator; Mar. 1995

NIFS-346 S. Sasaki, S. Takamura, S. Masuzaki, S. Watanabe, T. Kato, K. Kadota,
Helium I Line Intensity Ratios in a Plasma for the Diagnostics of Fusion Edge Plasmas; Mar. 1995

NIFS-347 M. Osakabe,
Measurement of Neutron Energy on D-T Fusion Plasma Experiments; Apr. 1995

NIFS-348 M. Sita Janaki, M.R. Gupta and Brahmananda Dasgupta,
Adiabatic Electron Acceleration in a Cnoidal Wave; Apr. 1995

NIFS-349 J. Xu, K. Ida and J. Fujita,
A Note for Pitch Angle Measurement of Magnetic Field in a Toroidal Plasma Using Motional Stark Effect; Apr. 1995

NIFS-350 J. Uramoto,
Characteristics for Metal Plate Penetration of a Low Energy Negative Muonlike or Pionlike Particle Beam: Apr. 1995

NIFS-351 J. Uramoto,
An Estimation of Life Time for A Low Energy Negative Pionlike Particle Beam: Apr. 1995

NIFS-352 A. Taniike,
Energy Loss Mechanism of a Gold Ion Beam on a Tandem Acceleration System: May 1995

NIFS-353 A. Nishizawa, Y. Hamada, Y. Kawasumi and H. Iguchi,
Increase of Lifetime of Thallium Zeolite Ion Source for Single-Ended Accelerator: May 1995

NIFS-354 S. Murakami, N. Nakajima, S. Okamura and M. Okamoto,
Orbital Aspects of Reachable β Value in NBI Heated Heliotron/Torsatrons; May 1995

NIFS-355 H. Sugama and W. Horton,
Neoclassical and Anomalous Transport in Axisymmetric Toroidal Plasmas with Electrostatic Turbulence; May 1995

NIFS-356 N. Ohyabu
A New Boundary Control Scheme for Simultaneous Achievement of H-mode and Radiative Cooling (SHC Boundary); May 1995